POD AND DMD OF FLOW NEAR SIDE SURFACE OF 2-D BLUFF BODY

Hiromichi Shirato, Yusuke Taniguchi, Ikuma Tsukamae and Mai Shimonishi
Department of Civil and Earth Resources Engineering, Kyoto University, Kyoto, Japan

Proper Orthogonal Decomposition (POD) and Dynamic Mode Decomposition (DMD) are to be applied to the flow near the leading edge and wake of a 2-D rectangular prism. Flow around 2-D rectangular prisms with B/D=1 and 8 are visualized by PIV and its 2-D velocity vector field is decomposed by POD and DMD. The prism is set in still condition in smooth flow and in grid turbulence in wind tunnel. Flow field in *xy* or *xz* plane (*x*: chord-wise, *y*: span-wise, *z*: vertical (normal to side surface) directions) is visualized using laser sheet and smoke under Re=2.5 to 3.75e3 with respect to D. DMD was applied to the wake behind a 2-D square prism at first examined. The periodicity in wake is clearly extracted by POD and DMD. Flow in a separation bubble is then observed through POD and DMD, which illuminate 3-dimensional flow characteristics and may connect with the increase of span-wise correlation of aerodynamic force.

Keyword: Wake, Separation bubble, POD, DMD.

1. INTRODUCTION

The conventional buffeting analysis proposed by Davenport[1)] is widely accepted in the wind loading codes for engineering structures including long span bridges and high-rise buildings. The analysis assumes that the span-wise coherence of aerodynamic force due to wind turbulence, gust force, is identical to that of oncoming wind velocity fluctuations. On the other hand, previous study reports that pressure fluctuations on a side surface of a still rectangular prism and resulting buffeting force shows higher span-wise coherence than that of oncoming flow[2)-9)]. Its mechanism has been understood as the distortion of approaching turbulent eddies at the leading edge and their elongation along span-wise direction[2), 9)], by the flow separation which has higher uniformity along span-wise direction[5)-7)], or due to 2-D like shedding vortices behind a bluff body for relatively smaller side ratio B/D (B: chord length, D: depth of cross section)[8)]. The authors' group has been investigating spatial correlation of surface pressure on the side surface of rectangular prisms in grid turbulence. In addition to the aforementioned higher span-wise correlation than the approaching wind, it was known that the surface pressure shows most correlated where the rms of pressure fluctuation reaches the maximum, then decreases near the reattaching point. Even in the region downstream from the reattaching point, the span-wise correlation has a tendency to increase again. The spatial correlation of the shear flow being separated from the leading edge was also discussed in wind tunnel experiments. Span-wise and chord-wise coherence of surface pressure were obtained for rectangular prisms for various side ratio B/D in three different grid turbulence. Based on these coherence data, a generalized frequency transfer function was proposed, which is equivalent to the multiple of joint mode acceptance and aerodynamic admittance[10)]. Surface pressure correlation between at the reference point near the leading edge and at the other point demonstrates more correlated tendency if the other location is not at along just downstream from the reference point but at along skewed direction from the main flow.

In this study, a new approach to capture the flow which enhances the span-wise correlation in the separation bubble on a rectangular prism with B/D=1 and 8 is attempted by implementing POD and DMD analysis to the time dependent PIV data of wind velocity field within the plane parallel to the side surface of a prism near the leading edge. In some POD modes, a ridge which expresses similar harmonic motion is recognized as expanding with a skew angle to the main flow direction. This implies cross momentum transport, that is transport of u-momentum towards span-wise direction by v-component and of *v*-momentum

[+1]isfa0001@jaxa.jp, [+2]isfa0002@company.com, [+3]isfa0003@univ.ac-u.jp

towards chord-wise direction by *u*-component, respectively. And this may create higher correlation of surface pressure at two locations with oblique angle to the main flow. Some DMD modes indicate little decaying rate and demonstrates enough sustainability. These modes may also an indication to provoke the cross momentum transport nature, since the domain of similar harmonic motion was observed with an oblique angle.

2. EXPERIMENTAL SETUP AND DATA DECOMPOSITION

(1) Wind Tunnel Experiment

A flat rectangular prism with B/D=8.0 (B=300mm, D=37.5mm and span length l=900mm) and a square prism (B/D=1) are focused in this study. The separating shear layer is expected to completely reattach to the side surface for B/D=8 and periodic Karman vortex shedding will be obtained for B/D=1. The prism is set horizontally and in still condition in the working section of wind tunnel. On the side surface of B/D=8 prism, 20 pressure taps are installed in one row along chord-wise direction and 13 rows are arranged in span-wise direction. Surface pressures are led to both ends of the prism through interior tubes in the model. The arrangement of pressure taps on the side surface is shown in Figure 1. Pressure signals are detected by 32ch multiple pressure transducers (ZOC17, Scanivalve) and stored in PC through A/D converter (DF-3422, Pavec) by 1kHz sampling rate.

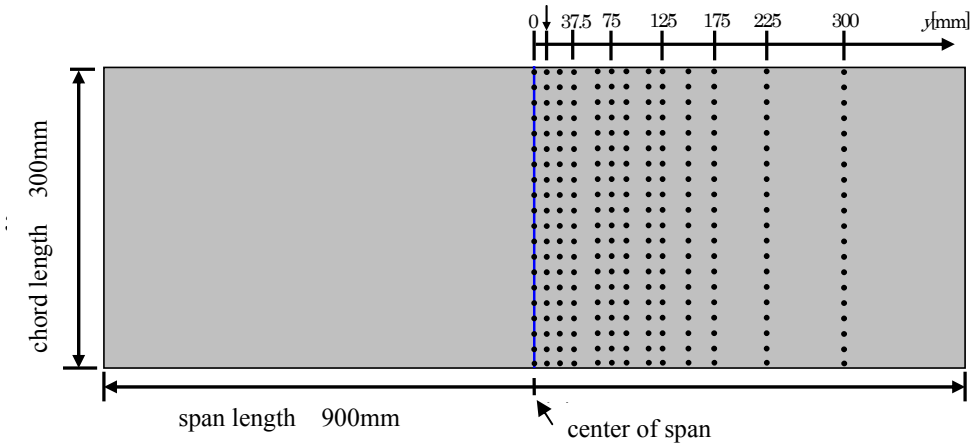

Figure 1: pressure tap arrangement of B/D=8 prism

The working section of the wind tunnel has 1000mm in width and 1800mm in height. Wind velocity is controlled over 0.5 to 25m/s continuously by adjusting constant rotation rate of fan. A grid consists of a bar 40mm in width (facing to main wind direction) with 160mm x 160mm square opening is installed at 2600mm (=8.67B) upstream from the prism to generate turbulent flow. Basic turbulence properties are summarized in Table 1. The scale of turbulence was evaluated by integrating the autocorrelation coefficient of longitudinal and vertical wind velocity fluctuation component. Wind velocity is measured by a hot-wire anemometer (model 1011, model 1013, Kanomax) with X-type probe (model 0252-T5, Kanomax) Figure 2 shows the experimental setup in wind tunnel.

Flow visualization is also carried out using laser sheet (PIV Laser 2000m/G-KD, Kato Koken) and smoke (model 8384, Kanomax)in order to obtain time dependent PIV data of wind velocity field within the plane parallel to the side surface of a prism near the leading edge. A PIV camera (Fastcam 1024PCI model 1K , Photoron) is used to capture the visualized image. The area to be visualized is 62.5mm in width (ly) and 150mm in length (lx) in xy plane (being horizontal and parallel to the side surface of a prism). The distance between side surface and the laser sheet is kept to 5mm (0.13D). Since the visualized area is immersed in the separation bubble, the smoke has to be supplied directly to the interior of the bubble. In this study, another identical prism as shown in Figure 3 is prepared, which has small slit near the leading edge so as to discharge the smoke. Wind velocity, U, is adjusted to 1.0m/s ($Re_D=UD/\nu$=2500) and 1.5m/s (Re_D=3750) in order to have

enough smoke density. As for the prism with B/D=1, B=D=37.5mm and the slit to emit smoke near the leading edge is installed on both sides. (See Figure 3)

Table 1: Basic properties of grid turbulence

Item	Component	Unit	Quantity
Intensity of turbulence	Longitudinal	[%]	10.5
	Vertical	[%]	9.0
Scale of turbulence	Longitudinal	[mm]	95.0
	Vertical	[mm]	45.0
Bar width		[mm]	60.0
Spacing distance		[mm]	160.0
Opening ratio		[%]	64.0

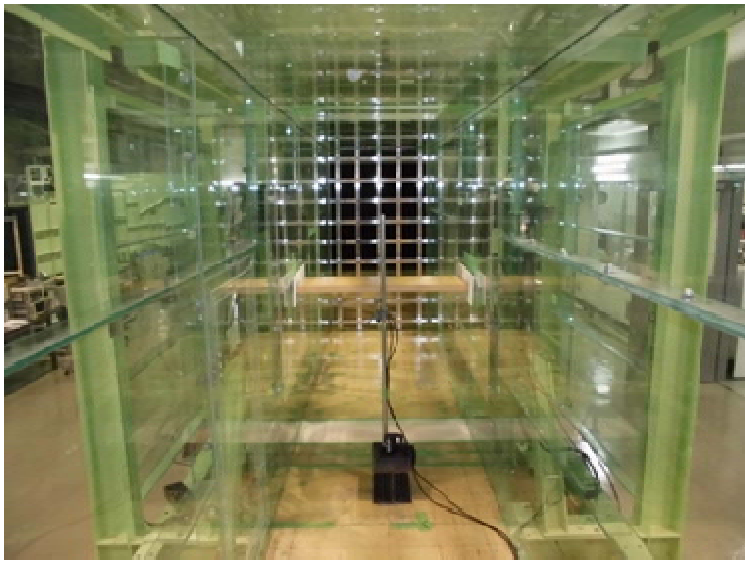

Figure 2: Experimental setup of a rectangular prism in grid turbulence

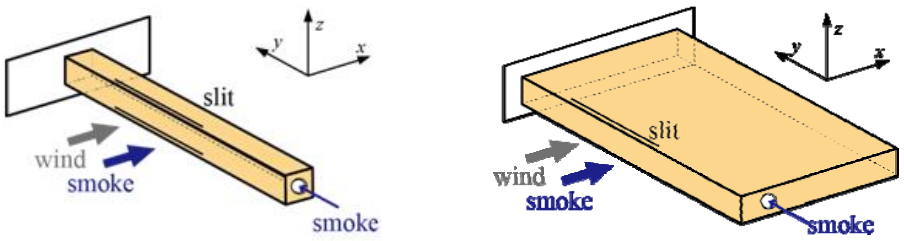

(a) B/D=1 (b) B/D=8

Figure 3: 2-D rectangular prism for flow visualization

(2) Mode Decomposition of Multivariate Time Series

a) POD

POD is widely used to extract dominating modes $\{\phi_r(\mathbf{x})\}$ (r=1, ..., n) of n-dof from m set of time series data (or m snap shots of image) of fluctuating components in a physical quantity $\{v_t(\mathbf{x})\}$ (t=0, Δt, $2\Delta t$, ..., $(m\text{-}1)\Delta t$), where Δt is constant sampling interval [sec]. A vector $\mathbf{x}$ denotes a certain location in n-dimensional space (or index of a certain node in 2-D plane), such as a velocity component at the location $\mathbf{x}$ [11)-14)]. A POD mode represents a principal steady flow structure fluctuating with its natural frequency. POD modes are determined by solving the eigenvalue problem of covariance matrix $[C]$ of $\{v_t(\mathbf{x})\}$, where the normalized eigenvectors of $[C]$ correspond the orthogonal POD modes and each eigenvalue represents energy contribution of a mode to the overall data. That is,

$$[C]\ \{\phi_r(\mathbf{x})\} \quad = \quad \lambda_r\ \{\phi_r(\mathbf{x})\} \tag{1}$$

$$\sum_{r=1}^{n} \int_{0}^{(m-1)\Delta t} [\{\phi_r(\mathbf{x})\}\ \{\phi_r(\mathbf{x})\}^T\ \{v_t(\mathbf{x})\}]^2 \quad dt \quad = \quad \sum_{r=1}^{n} \lambda_r \tag{2}$$

where, $[C]$: covariance matrix of time series data $\{v_t(\mathbf{x})\}$,

$$[C] = \frac{1}{T} \int_{0}^{(m-1)\Delta t} \{v_t(\mathbf{x})\}\{v_t(\mathbf{x})\}^T dt \tag{3}$$

$\{\phi_r(\mathbf{x})\}$: r-th POD mode (r=1, ..., n) and $\{\phi_i(\mathbf{x})\}\ \{\phi_j(\mathbf{x})\}^T = \delta_{ij}$ (Kronecker's delta), T: data length [sec].

b) DMD

DMD is able to extract temporal variation in the flow fields[14)] and gives temporal and spatial evolution of flow pattern. Phase information of velocity component at different location is also contained in DMD modes, whereas the ordinary POD loses it[15)]. DMD assumes that time sequence of physical quantity, $\{v_t(\mathbf{x})\}$ to $\{v_{t+\Delta t}(\mathbf{x})\}$, can be expressed by a linear mapping,

$$[A]\ \{v_t(\mathbf{x})\} = \{v_{t+\Delta t}(\mathbf{x})\} \tag{4}$$

where, $[A]$ is a matrix and not a function of time t.
An m set of time series data, $[\boldsymbol{X}]_0^{(m\text{-}1)\Delta t}$, can be converted to $[\boldsymbol{X}]_{\Delta t}^{m\Delta t}$ by using $[A]$,

$$\begin{aligned} [A]\ [\boldsymbol{X}]_0^{(m-1)\Delta t} \quad &= \quad [[A]\{v_0(\mathbf{x})\}, [A]\{v_{\Delta t}(\mathbf{x})\}, [A]\{v_{2\Delta t}(\mathbf{x})\}, ..., [A]\{v_{(m-1)\Delta t}(\mathbf{x})\} \\ &= \quad [X]_{\Delta t}^{m\Delta t} \end{aligned} \tag{5}$$

where, $[\boldsymbol{X}]_0^{(m\text{-}1)\Delta t} = [\{v_0(\mathbf{x})\}, \{v_{\Delta t}(\mathbf{x})\}, \{v_{2\Delta t}(\mathbf{x})\}, ..., \{v_{(m-1)\Delta t}(\mathbf{x})\}]$.
DMD modes are eigenvectors of the matrix $[A]$. Instead of solving eigenvalue problem of $[A]$ directly, the mathematical approach called singular value decomposition (SVD) will be used because of saving time to solve large-scale eigenvalue analysis and the SVD gives more robust result[14), 15)]. By SVD, the matrix $[\boldsymbol{X}]_0^{(m\text{-}1)\Delta t}$ can be decomposed into three matrices $[U]$, $[\Sigma]$ and $[W]$, as

$$[\boldsymbol{X}]_0^{(m-1)\Delta t} \quad = \quad [U][\Sigma][W]^* \tag{6}$$

where, $[U]$ and $[W]$ are unitary matrices, $[\ ]^*$ is the transposed taking conjugate of each element.
Substituting equation (6) into equation (5), the matrix $[S]$ can be obtained after rearranging,

$$[S] = [U]^*[A][U] = [U]^*\ [\boldsymbol{X}]_{\Delta t}^{m\Delta t}\ [W][\Sigma]^{-1} \tag{7}$$

All matrices in the right hand side of equation (7) can be calculated or available, the matrix [S] is determined. Since the matrix [A] contains the POD modes of the data sequence $[\boldsymbol{X}]_0^{(m-1)\Delta t}$, the above operation amounts to a projection of the linear operator [A] onto a POD basis [15]. Eigenvectors of [A], DMD modes, are calculated from eigenvectors of the matrix [S] as

$$\{\xi_r\} = [U]\{y_r\} \tag{8}$$

where, $\{\xi_r\}$: r-th DMD mode, $\{y_r\}$: r-th eigenvector of [S], i.e. $[S]\{y_r\} = \kappa_r\{y_r\}$.

The data $\{v_{m\Delta t}(\mathbf{x})\}$ can be expressed as:

$$\{v_{m\Delta t}(\mathbf{x})\} = [A]^{m-1}\{v_0(\mathbf{x})\} = \sum_{r=1}^{n} c_r \kappa_r^{m-1}\{\xi_r\} \tag{9}$$

where, c_r is the coefficient decided for each mode and has a dimension of focused physical quantity (velocity [m/s] in this study).

The coefficient c_r is not a function of time (but degree of contribution), and only the part κ_r^{m-1} in equation (9) is dependent on time [14]. The norm of κ_r determines amplification of flow structures in the DMD mode, while the characteristic frequency of the DMD mode can be obtained by argument of κ_r as:

$$f_r = arg[\kappa_r]/2\pi/\Delta t \tag{10}$$

where, f_r: frequency of r-th DMD mode [Hz], $arg[\ ]$: argument of complex number ($arg[\ ] = \tan^{-1}(Im(\ )/Re(\ ))$.

Figure 4 compares the energy distribution of DMD modes determined by eq. (11) and PSD of vertical velocity (w-) component in the wake behind the B/D=1 prism.

$$F_{midr} = c_{midr}^2 = (c_r|\kappa_r|^{m/2})^2 \tag{11}$$

where, F_{midr}: energy of r-th DMD mode at $t=m\Delta t/2$ assuming the data consists of m snap shots with sampling interval of Δt.

It is known that the energy distribution of F_{mid} is similar to PSD and the frequency at the peak in the figure corresponds well to the vortex shedding frequency. Figure 5 shows the time evolution of a DMD mode of wake behind the B/D=1 prism, whose characteristic frequency is the same as that of vortex shedding. The organization with alternating sign is moving toward downstream and this mode captures well the dominating periodic flow. And DMD is one of the powerful tools to extract dominating and sustainable modes from complex flow pattern.

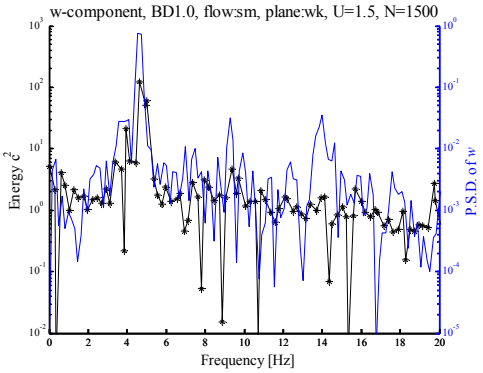

Figure 4 Comparison of energy distribution of DMD mode and PSD of w-component in wake (B/D=1).

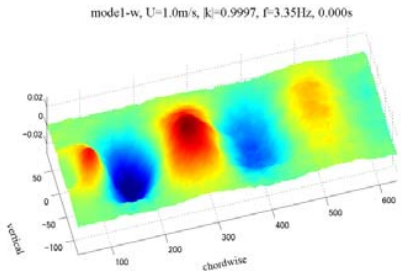

$\omega t = 0$

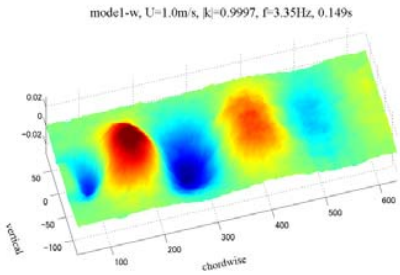

$\omega t = \pi$

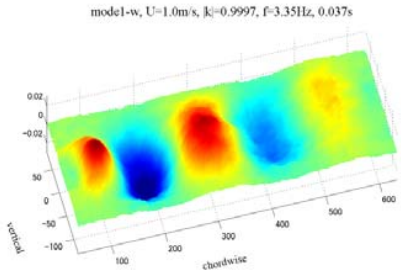

$\omega t = 1/4\ \pi$

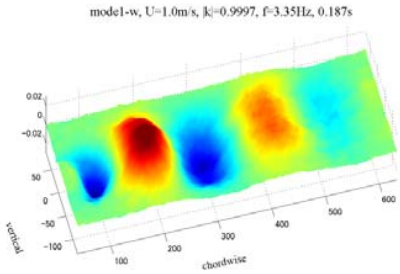

$\omega t = 5/4\ \pi$

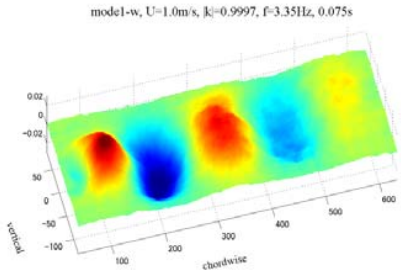

$\omega t = 1/2\ \pi$

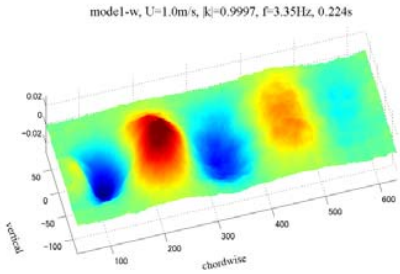

$\omega t = 3/2\ \pi$

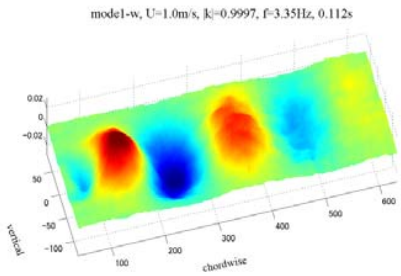

$\omega t = 3/4\ \pi$

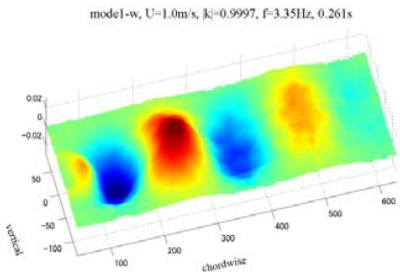

$\omega t = 7/4\ \pi$

Figure 5 time evolution of DMD mode in wake (B/D=1).

3. RESULTS AND DISCUSSION

(1) Pressure fields of side surface

Time averaged and *rms* of pressure coefficients, C_{p_bar} and C_{p_tilder}, at each pressure tap on the side surface are shown in Figure 6. The reattaching point of separating flow is presumed to be at around x/D=1.8 to 2.6, by taking an indication of "a bit downstream from C_{p_tilder} peak and a bit upstream of C_{p_bar}" by the literature.

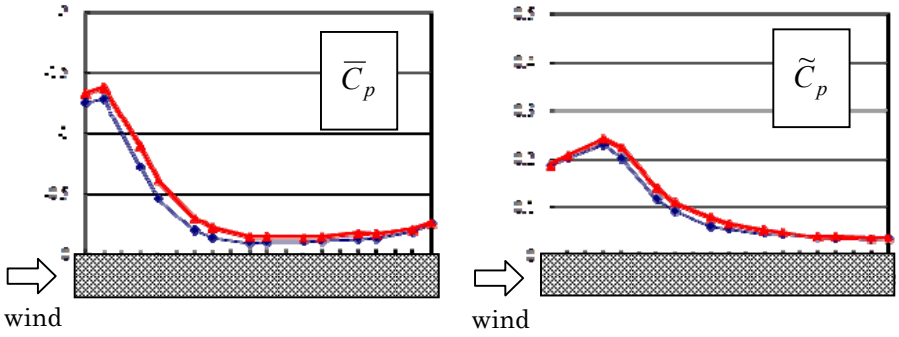

Figure 6: Time average and rms of pressure coefficient (B/D=8.0 rectangular prism in grid turbulence)

Figure 7 shows spatial distribution of cross correlation coefficient of surface pressure fluctuation between two locations on the side surface. Reference point is chosen at the most upstream pressure tap in the span center of the prism (indicated by red solid circle in the figure). Cross correlation coefficient $\rho_p(x,y)$ is calculated by the following equation:

$$\rho_p(x, y) = E[p(x_0, y_0; t)p(x, y; t)] / [\{E[p(x_0, y_0; t)^2]\}^{1/2}\{E[p(x, y; t)^2]\}^{1/2}] \quad (11)$$

where, $E[f(t)g(t)]= \frac{1}{T}\int_0^T f(t)g(t)dt$, T: data length [sec], $p(x_0, y_0; t)$: time series of pressure fluctuation at the reference point [Pa], $p(x, y; t)$: time series of pressure fluctuation at location (x, y) [Pa].

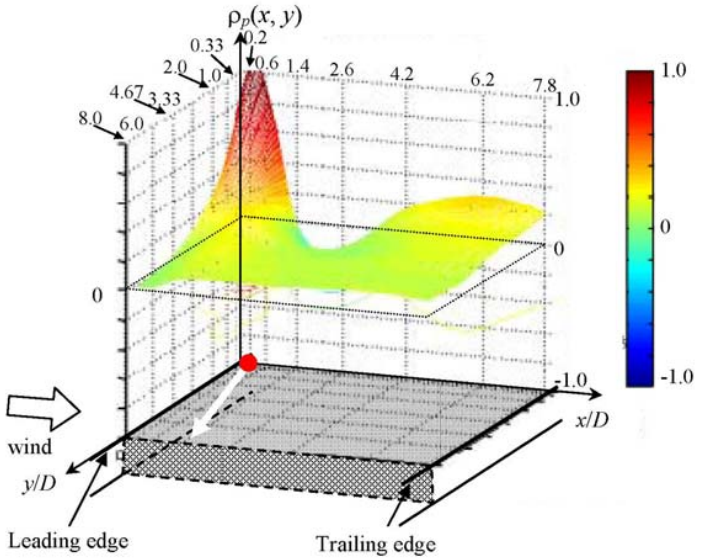

Figure 7: Spatial distribution of cross correlation coefficient $\rho_p(x/D, y/D)$
(● : reference point, $(x_0/D, y_0/D)$=(0.2, 0). White arrow indicates relatively more correlated domain.)

The cross correlation coefficient takes negative value at about x/D=1.4 to 3.5 and just downstream from the reference point. This region is presumed to be near the reattaching point. This negative correlation means that the pressure in this region fluctuates out of phase from those at the reference point. If the location of reattaching point is assumed to move back and forth, the separation bubble will undergo shrink and elongation. Pressure level in the separation bubble will be up and down alternatively. When the bubble shrinks, the reattaching point must move to upstream and pressure level in the bubble will decrease. Therefore, pressure at the reference point being always in the bubble will be more negative, while pressure at near the reattaching point will be out from the bubble which makes pressure reduced (relatively more positive).

It is known that the pressure near the leading edge and being apart from the reference point more than 4.67D shows almost non-correlated. However, along the line parallel to x axis at y/D=8.0, the coefficient starts from zero near the leading edge but seems to increase and slightly more positive value. It seems that the distribution of cross correlation coefficient displays more correlated domain along the white arrow as shown in the figure. The existence of this skewed correlated domain was confirmed for other rectangular prisms with different B/D as shown in Figure 8 and in other grid turbulence.

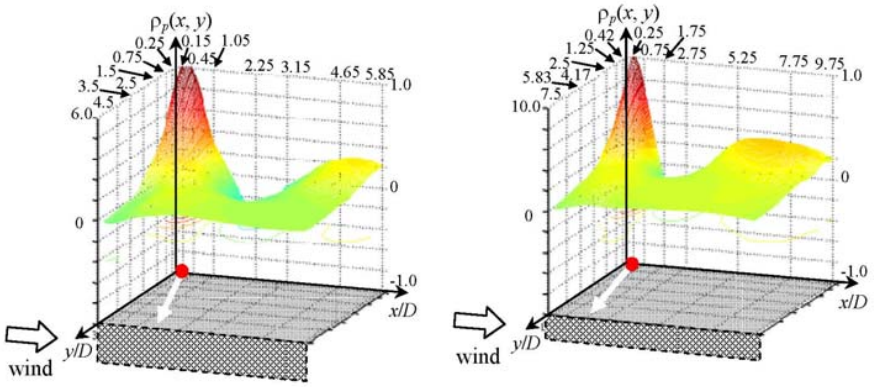

(a) B/D=6.0 (b) B/D=10.0

Figure 8: Spatial distribution of cross correlation coefficient $\rho_p(x/D, y/D)$

(2) Velocity fields on side surface

Figure 9 shows the 1st and 2nd POD modes for u and v components in xy plane. For both components, the 1st mode looks to be relatively uniform along span-wise direction, whereas the non-uniform pattern dominates in the 2nd mode. The energy ratio of the 1st mode to the 2nd is about 3 for u- and 2 for v-component, where the participation of the 1st mode to the overall variance is 6% for u- and 4% for v-component. Therefore, the entire velocity field cannot be well described by the 1st mode only, and the 2nd or higher mode plays an important role. Larger u-component appears in x/D=2.5 to 3.5, which is just behind the reattaching point at around x/D=1.8 to 2.6 presumed in the last sub-section, (1). This area invokes the longitudinal movement of the reattaching point in back and forth manner.

It may be pointed out that there is a skewed ridge configuration in the 2nd mode and more typical in v-component, in this case. The u-momentum in the ridge may be transported towards span-wise direction by v-component and of v-momentum towards chord-wise direction by u-component. This cross momentum transport will enhance the mixing of flow and will contribute to the increase of span-wise correlation of velocity components as well as surface pressure.

Figure 10 is obtained by DMD. Since each DMD mode (eigenvector) consists of complex number elements, it is not easy to catch an image of dynamic flow patterns from DMD modes by displaying real part or norm (absolute value) of each element of an eigenvector. The figures indicated below are displaying phase lag between at the reference point ate the leading edge (at bottom left by black circle) and each location in the domain, which is determined by:

$$\psi_r(x, y) = \arg[\{\xi_r\}_i] - \arg[\{\xi_r\}_{ref}] \quad (12)$$

where, $\psi_r(x, y)$: phase lag of the r-th DMD mode at (x, y), $\{\xi_r\}i$: the i-th element of the r-th DMD eigenvector which corresponds to the location at (x, y), $\{\xi_r\}_{ref}$: the element corresponding to the reference point.

The two modes (4th and 32nd) are selected under the condition of small enough decaying rate ($|\kappa_r|$=0.972 for 4th, 0.995 for 32nd) and low natural frequency (f_r =3.67[Hz] for 4th, 8.80[Hz] for 32nd). Small decaying rate, $|\kappa_r|$ being nearly equal to 1.0, represents enough sustainability of these modes. As for the 4th DMD mode, wide area having the same phase lag is scattered at x/D=2.8 to 4.0 (within the broken line in the figure), where larger velocity component was observed in the POD 1st mode as shown in Figure 8. Furthermore, the skewed area of the same phase lag is obtained in the 32nd DMD mode within the broken line. This may be again an indication of the cross momentum transport and the increase of span-wise correlation.

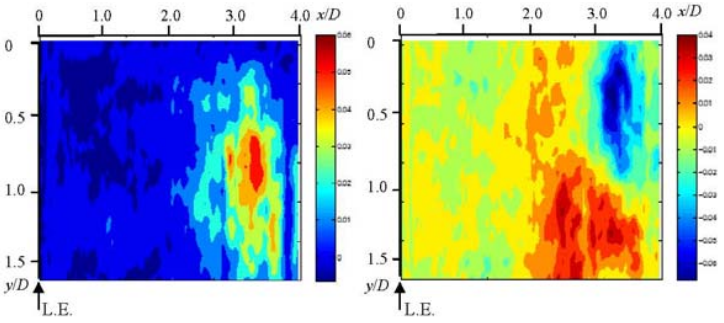

(a) *u*-component

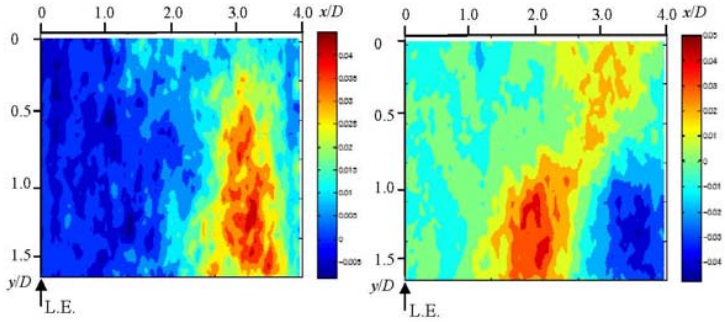

(b) *v*-component

Figure 9: POD modes for u- and v-velocity components
(left: 1st mode, right: 2nd mode, The entire flow direction is from left to right)

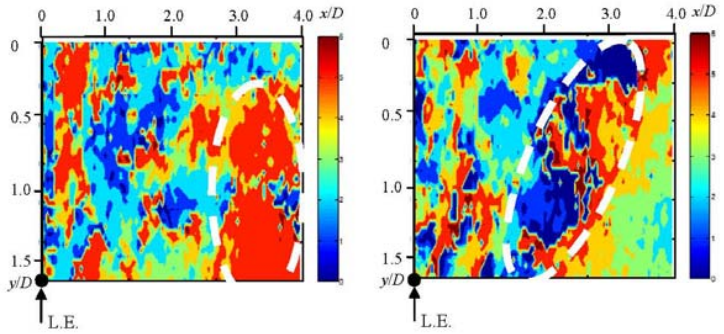

Figure 10: Phase lag from the reference point (indicated by black circle)
(*v*-component, left: 4th mode, right: 32nd mode)

4. CONCLUDING REMARKS

Some remarks to conclude are listed as follows:

(1) A domain with skew angle to the main flow was observed in the cross correlation coefficient, where the correlation was relatively higher. This implies the cross momentum transport and contributes to the increase of span-wise correlation.

(2) POD and DMD were applied to the 2-D velocity field near the side surface. Some mode shapes were not in parallel to the leading edge but skewed. This may supports the above observation in the pressure field.

ACKNOWLEDGMENT

Special thanks to Mr. Yutaro Kawata (Obayashi Corp. (former graduate student)) for his pioneering research on DMD.

REFERENCES

1) A. G. Davenport, “A statistical approach to the treatment of wind loading on tall masts and suspension bridges”, Ph.D. Dissertation, Univ. of Bristol, 1961

2) G. L. Larose, “The span-wise coherence of wind forces on streamlined bridge decks”, Proc. of the 3rd International Colloquium on Bluff Body Aerodynamics and its Applications, 1996.

3) J. B. Jakobsen, “Span-wise structure of lift and overturning moment on a motionless bridge girder”, Journal of Wind Engineering and Industrial Aerodynamics, 69-71, 795-805, 1997.

4) K. Kimura, Y. Fujino, S. Nakato, H. Tamura, “Characteristics off buffeting forces on Flat Cylinders”, Journal of Wind Engineering and Industrial Aerodynamics , 69-71, 365-374, 1997

5) M. Matsumoto, H. Shirato, K. Araki, T. Haramura, T. Hashimoto, ” Spanwise coherence characteristics of surface pressure field on 2-D bluff bodies”, Journal of Wind Engineering and Industrial Aerodynamics, vol.91(1-2), 155-163, 2003.

6) M. Matsumoto, H. Shirato, T. Haramura, Y. Odawara. “Spanwise coherent structure of surface pressure on a 2-D bluff body in turbulent flow”, Proceedings of the 11th International Conference on Wind Engineering, Lubbock, Texas, 681-688, 2003.

7) H. Shirato and M. Matsumoto, “Temporal and Spatial Correlated Properties of Surface pressure and gust forces on a rectangular section in vertical fluctuating winds”, Journal of Structural Engineering A, JSCE, 162(3), 669-680, 2006 (in Japanese).

8) Y. Ito, H. Shirato, M. Matsumoto, “Span-wise correlations of fluctuating lift forces on 2D rectangular cylinders”, Journal of Wind and Engineering, vol.11, No.2, pp.1-10, 2014.

9) J. C. R. Hunt, “Turbulent Velocities near and Fluctuating Surface Pressures on Structures in Turbulent Winds”, Proceedings of the 4th International Conference on Wind Engineering, pp.309-320, 1975.

10) H. Shirato, Y. Sato, O. Sasaki, A. Mahindra and R. Mitsugi, “Surface pressure correlation and buffeting force evaluation”, Proceedings of the 13th International Conference on Wind Engineering, Amsterdam, 2011.

11) Y. Tamura, H. Ueda, H. Kikuchi, K. Hibi and B. Bienkiewics, “Proper orthogonal decomposition study of approach wind – building pressure correlation”, Proceedings of the 9th International Conference on Wind Engineering, Retrospect and Prospect, vol.IV, pp.2115-2126, 1995.

12) L. Carassale, G. Solari and F. Tubino, “Proper orthogonal decomposition in wind engineering, Part 2: Theoretical aspects and some applications”, Wind & Structures, 10(2), pp.177-208, 2007.

13) K. Taira, “Proper Orthogonal Decomposition in Fluid Flow Analysis: 1. Introduction”, Nagare, 30, pp.115-123, 2011 (in Japanese).

14) M. Sakai, Y. Sunada, T. Imamura and K. Rinoie, “Experimental and Numerical Flow Analysis around Circular Cylinders Using POD and DMD”, AIAA Fluid Dynamic Conference, pp.1-19, 2014.

15) P. J. Schmid, “Dynamic mode decomposition of numerical and experimental data”, Journal of Fluid Mechanics, vol.656, pp.5-28, 2010.